# Developments in the Dynamical Theory of High Energy Electron Reflection

Y. MA AND L.D. MARKS
*Materials Research Center, Northwestern University, Evanston, Illinois 60208*

*ABSTRACT*    High energy electron reflection (HEER) is an important technique in surface science and uses the information carried by high energy electrons reflected from surfaces to study surface structures and surface electronic states. With the development of reflection high energy electron diffraction (RHEED), high energy electron microscopy (REM), and high energy electron energy loss spectroscopy (EEL) in surface science, the usefulness of HEER has been widely recognized and demonstrated. However, a stationary dynamical solution for an arbitrary surface for HEER has not been obtained yet.

In this paper, some developments in understanding the dynamical theory of HEER, particularly in recent years, are reviewed:

1. The introduction of the concept of current flow for a semi-infinite crystal model has removed the confusion around the wave points in the "band gap."
2. The consistency between the Bloch wave and multislice in the Bragg case has verified the validity of the argument of current flow and led to the emergence of the BMCR method (Bloch wave + Multislice Combined for Reflection).
3. The failure of the Bloch Wave-Only solution (the BWO solution) on Au (110) surfaces in the Bragg case revealed by the BMCR method implies that previous BWO calculations in the Bragg case might be at fault.
4. The 2-D dependence of the electron wave fields and Picard iteration-like character of multislice calculation in the Bragg case has led to the emergence of an Edge Patching method in Multislice-mode-Only (the EPMO method). The new method yields an infinitely convergent stationary dynamical solution for an arbitrary surface.

## INTRODUCTION

High energy electrons reflected from a crystal surface can be used for surface investigations in both real space (reflection high energy electron microscopy, REM) and reciprocal space (reflection high energy electron diffraction, RHEED), and the energy can also be analyzed to obtain information about surface electronic states (reflection high energy loss spectroscopy, EEL). The combination of these approaches has proved to be a powerful tool to study the structure and electronic states of crystal surfaces and the correlation between the two. The advantages of using reflected high energy electrons can be listed as: 1) short wavelength and high resolution in images; 2) high surface sensitivity for small glancing incident angle; and 3) ability of modern techniques to combine the three different approaches together in the microscope, which will lead to a combination of surface science and traditional electron microscopy.

With the recent development of ultra-high vacuum (UHV) techniques and electron optical systems, there has been a revival of interest in HEER, as opposed to low energy electron reflection (LEED) which is also used for both imaging (REM) and diffraction (LEED). Experimentally, the new revival has been enhanced by the studies of surface features using high resolution

REM and developments in the studies of molecular beam epitaxy (MBE) using RHEED patterns.

## HISTORIC REVIEW OF HIGH ENERGY ELECTRON REFLECTION (HEER)

Since 1933, when Ruska first imaged the surface of solids with high energy electrons reflected from the surface, REM has experienced an unsteady development (Borries, 1940; Fert and Saport, 1952; Menter, 1953). This is due to the competition of other surface imaging techniques, such as the replica technique for transmission electron microscopy (TEM), scanning electron microscopy (SEM), and now scanning tunneling microscopy (STM).

Interest in REM was revived in the 1970's by Cowley and Hojlund Nielsen (1975; Hojlund Nielsen and Cowley, 1976) with the emphasis put on diffraction contrast combining both reciprocal space and real space analyses. Since then, REM experiments have been done with

---

ordinary as well as specially modified UHV electron microscopes. The types of specimens studied include metals, semiconductors, and insulators (Hsu, 1983; Hsu and Cowley, 1983; Hsu et al., 1984; Osakabe et al., 1980, 1981a, b; Shimizu et al., 1985, 1987; Uchida et al., 1984a, b). More detailed investigations on various crystal surfaces by REM are continuously reported (Lehmpfuhl and Uchida, 1988; Uchida and Lehmpfuhl, 1987a, b; Yao and Cowley, 1988).

Unlike REM, since Nishikawa and Kikuchi (1928a, b) first obtained the RHEED pattern, the development of RHEED technique has been rather steady. This is mainly because in many cases it is used with a simple RHEED camera instead of being associated with a complicated electron optical system.

The usefulness of RHEED was recognized from its early applications in surface studies, such as oxide films on crystal surfaces, metal films formed by liquid phase epitaxy (LPE) (Miyake, 1937a, b; Uyeda, 1940), and surfaces covered by organic molecules (Kainuma and Uyeda, 1950). Since then RHEED has been widely used in surface science as an alternative technique to LEED for studying surface reconstruction, nucleation, crystallization, varied surface features, and the mechanism of crystal growth (Bertrand et al., 1985; Cohen et al., 1986; Houzay et al., 1984; Ino, 1977; Pukite et al., 1987). An impressive development in RHEED was made by Ino's group (Gotoh and Ino, 1978; Ino, 1980). The RHEED patterns taken by Ino et al. are much clearer and more informative than any other obtained before and reveal the full power of RHEED for surface investigation.

A recent important development in RHEED was the discovery of the correlation between intensity oscillation in RHEED pattern and crystal growth on a surface during molecular beam epitaxy (MBE) (Harris et al., 1981a, b; Wood, 1981). Because the periodicity of oscillation in all observations corresponds exactly to the growth of a single monolayer, it provides an absolute measurement of the growth rate.

Another new development in RHEED is spot splitting which was first observed in RHEED half a century ago (Nishikawa and Kikuchi, 1928a, b). Pukite et al. used sensitive measurements of the RHEED spots to show that the spot splitting is related to both the vicinal angle of surfaces and incidence azimuth (Pukite et al., 1983; Pukite and Cohen, 1987).

## HISTORIC REVIEWS ON DEVELOPMENT OF DYNAMICAL THEORY FOR HEER

With the development of HEER techniques, tremendous efforts have been put into the development of dynamical theory for HEER. However, compared to electron transmission, the development of a dynamical theory for electron reflection has been slow. This is largely due to the complexity of the boundary value problem and the nature of the Bloch wave in the Bragg case. Like the dynamical theory for high energy electron transmission (TEM), the early development of dynamical theory for HEER was based upon the Bethe theory (or Bloch wave method) (Bethe, 1928). The Bloch wave method uses a plane wave expansion to convert the Schrodinger equation in real space into one

in momentum space which is also a dispersion equation defining the E-k relation. The difference between energy band theory and Bloch wave theory for electron diffraction is which variable, E or **k**, is taken as an independent variable in the E-**k** relation (E is the total energy of an electron in a given system and **k** the crystal momentum).

Since the earliest development of HEER techniques, the Bethe theory has been widely applied for interpretation of phenomena in RHEED (Kawamura et al., 1976; Kohra, 1962; Miyake et al., 1954). However, for a long time, the way of handling a complex dispersion surface and the wave points in the "band gap" was a problem. In the 1970's, Colella (1972), Colella and Menadue (1972), and Moon (1972) introduced an alternative way of applying the Bloch wave method to electron reflection. To avoid the dilemma of determining excited wave points on a complex dispersion surface, an additional bottom boundary was introduced. The method has two disadvantages: 1) The computation speed slows down by introducing a 2N × 2N matrix (N the number of reciprocal lattice points included) and one additional bottom boundary. 2) The physical mechanism of reflection is concealed in the numerical processes. There are also two methodical problems for the approach: 1) The crystal potential is truncated at the top atomic layer while a real surface potential exponentially extends into vacuum. This was later discussed by Britze and Meyer-Ehmsen (1978) using the WKB method. 2) The surface sensitivity of HEER cannot be taken into account. The Bloch wave method basically is one for bulk phenomena since it always takes a crystal as infinite or semi-infinite bulk, while both experimental and numerical investigations have shown that HEER is highly sensitive to the structure of the first few atomic layers.

The Bloch wave method in principle is only suitable for a perfect and periodic crystal, while a lot of surface phenomena result from surface imperfections, such as surface steps, clusters, dislocations, reconstructions, relaxations, and a surface potential. This means that it is necessary to find alternative methods which are adapted to surface imperfections. Borrowing the concept of slice used by Darwin (1914) for X-ray diffraction and Howie and Whelan (1977) for TEM, Maksym and Beeby (1981) developed a method for electron reflection in which a crystal is considered perfect and periodic in a plane parallel to the surface, and non-periodic modulation of the potential only occurs in the direction normal to the surface. Therefore, we here call it a "parallel multislice" method to distinguish it from later discussed "vertical multislice" methods. The limitation of the approach is that it is inherently unsuitable for calculating reflection waves from the crystal defects involving structural variation in a plane parallel to the crystal surface, and the sampling rate along the direction normal to the surface and incident beam is low. In addition, the physical insights of electron reflection are generally not available for the method. Another multislice approach for reflection dynamical calculation introduced by Peng and Cowley (1986, 1988) was based upon the multislice formulation developed by Cowley and Moodie (1957, 1959a, b). Here, the slices of crystal

are taken normal to the surface as they are for profile image simulations for TEM. Therefore, we call it a "vertical multislice" method. Because there is no restriction on the way of constructing the phase grating of slices, it is possible to include any desired modification of the surface structure, and surface potential is also automatically included in the phase grating. This is the most significant feature of the method. However, edge effects inherently stand in the way of getting a stationary solution and limit its application to real problems in HEER. In addition, like other numerical methods in which the physics usually is concealed by numbers, this method is also not convenient for exploring the physical insights of HEER.

## BLOCH WAVE METHOD FOR HEER

The idea behind exploiting the Bloch wave method for HEER is to combine the Bloch wave method and the "vertical multislice" method to overcome the disadvantages of the two individual methods: the inconvenience for surface imperfections of the Bloch wave method and the edge effects of the multislice.

For electron reflection from a crystal surface, a physically correct model is a semi-infinite crystal model. However, this model encounters a decades-long dilemma: how to determine excited wave points on a complex dispersion surface. For a semi-infinite crystal, the number of excited wave points, i.e., excited Bloch waves, should be no more or no less than the number of reciprocal lattice points included: N. Mathematically, a semi-infinite crystal only has one boundary with vacuum, which gives 2N equations for the continuity of the wave function and the derivative of the wave function. Therefore, only N Bloch waves can be included, otherwise the problem has no unique solution. Note that the number of possible Bloch waves from the dispersion equation (E-k relation) is always 2N. Physically, for a semi-infinite crystal, there should be no back reflections from the bottom boundary. There are two critical questions: 1) how to define a Bloch state as a "forward state" or "backward state," and 2) whether the number of the "forward" or "backward" states is N or not. Several authors (Kawamura et al., 1976; Kohra et al., 1962; Miyake et al., 1954) have discussed the role of energy flow in this problem, but no detailed approach was given. This problem can be solved by introducing the concept of current flow (Ma and Marks, 1989; Marks and Ma, 1989).

In general, the orientation of a wave is determined by its energy flow instead of its momenta. The energy flow of an electromagnetic wave is defined by the Poynting vector $S = (1/2)E \times H$ and is carried by the medium—electromagnetic field. A matter wave is interpreted as a wave of "probability," for which there is no medium, so the energy is carried by particles. Therefore, the probability current flow for a matter wave corresponds to the Poynting vector for an electromagnetic wave. The equivalence between the energy flow and current flow for a matter wave and the dispersion surface has been discussed in detail elsewhere (Ma, 1989).

The current flow of a Bloch wave can be easily derived analytically by substituting the wave function of a Bloch wave into the general form of the current flow of a matter wave (Ma and Marks, 1989; Marks and Ma, 1989):

$$S^{(j)} = (2\pi h/m)\exp[-4\pi k^{i(j)} \cdot r][\Sigma_g |C_g^{(j)}|^2 (k^{r(j)} + g)] \quad (1)$$

where $k^{r(j)}$ is the real part of the wave vector, $k^{i(j)}$ the imaginary part of the wave vector, $\{C_g^{(j)}\}$ the coefficients of a plane wave $g$. The superscript j denotes a specific excited Bloch state. Equation 1 shows that the current flow of a Bloch wave is proportional to the expectation value of its all possible wave momenta ($p = hk$), if the wave function is normalized: $\Sigma_g |C_g^{(j)}|^2 = 1$. The z component of S is given by

$$S_z^{(j)} = (2\pi h/m)\exp[-4\pi k_z^{i(j)}z][\Sigma_g | C_g^{(j)}|^2(k_z^{r(j)} + g_z)]. \quad (2)$$

If the z axis is set as the inward normal to the surface, the Bloch wave which physically exists in a semi-infinite crystal must satisfy $S_z^{(j)} \geq 0$ and $k_z^{i(j)} \geq 0$. This becomes the criterion for determining excited Bloch waves in a semi-infinite crystal.

The signs of $S_z^{(j)}$ and $k_z^{i(j)}$ can be used to characterize four kinds of different Bloch waves:

1. $V_I = 0$ (no absorption), $S_z^{(j)} = 0$, $k_z^{i(j)} = 0$; a non-evanescent standing wave in an ideal medium.
2. $V_I = 0$ (no absorption), $S_z^{(j)} = 0$, $k_z^{i(j)} \neq 0$; an evanescent standing wave in an ideal medium.
3. $V_I = 0$ (no absorption), $S_z^{(j)} \neq 0$, $k_z^{i(j)} = 0$; a non-evanescent propagating wave. Note that in the medium without absorption, there is no Bloch wave with $S_z^{(j)} \neq 0$ and $k_z^{i(j)} \neq 0$. In other words, there is no "evanescent propagating wave."
4. $V_I > 0$ (with absorption), $S_z^{(j)} > 0$, $k_z^{i(j)} > 0$ or $S_z^{(j)} < 0$, $k_z^{i(j)} < 0$; an evanescent standing wave or a non-evanescent propagating wave in the medium with absorption.

When absorption is introduced, the mechanism of evanescence and absorption are mixed with each other and both of them are characterized by $S_z^{(j)} > 0$ and $k_z^{i(j)} > 0$ or $S_z^{(j)} < 0$ and $k_z^{i(j)} < 0$. Table 1 shows the numerical results for a GaAs (001) surface for the case both with and without absorption. The beam direction is along the [010] Laue zone axis and 9 beams are included. For the absorption, the imaginary parts of the Fourier potential coefficients were taken as 10% of their real parts. The results indicate that in a medium with absorption, the magnitude of $k_z^{i(j)}$ for an evanescent wave is much larger than that for a non-evanescent Bloch wave since the decay of an evanescent wave is due to both the evanescent mechanism and the absorption in the evanescent region rather than only the absorption of a non-evanescent Bloch wave. The results also show that the number of Bloch waves satisfying the condition $S_z^{(j)} \geq 0$ and $k_z^{i(j)} \geq 0$ is exactly N both with and without absorption.

For the Laue case, the dynamical theory has not encountered the difficulty of determining excited wave points on dispersion surface and the requirement of the current flow analysis, because in the Laue case $|k_z^{r(j)}| >> |g_z|$ and $k_z^{i(j)} = 0$. These two relations result in $S_z^{(j)}k_z^{r(j)} > 0$, i.e., the orientation of current flow along

*TABLE 1. List of the Bloch waves for a 9-beam calculation for GaAs (001) surface*[1]

**ALL EXCITED BLOCH WAVES**

| | WITHOUT ABSORPTION | | | WITH ABSORPTION | |
|---|---|---|---|---|---|
| | EIGENVALUES $(k_{oz})$ | ENERGY FLOW $(S_z)$ | | EIGENVALUES $(k_{oz})$ | ENERGYFLOW $(S_z)$ |
| 1 | ( 0.73292+ 0.00000i); | 0.38051 | 1 | ( 0.73315+ 0.01586i); | 0.38066 |
| 2 | (-0.73292+ 0.00000i); | -0.38276 | 2 | (-0.73315+-0.01586i); | -0.38294 |
| 3 | ( 0.59945+ 0.00000i); | 0.26390 | 3 | ( 0.60116+ 0.03088i); | 0.26517 |
| 4 | (-0.59945+ 0.00000i); | -0.27529 | 4 | (-0.60116+-0.03088i); | -0.27645 |
| 5 | ( 0.35425+ 0.14888i); | 0.00000 | 5 | ( 0.37829+ 0.15073i); | 0.02119 |
| 6 | ( 0.35425+-0.14888i); | 0.00000 | 6 | ( 0.33023+-0.15093i); | -0.28858 |
| 7 | (-0.35425+ 0.14888i); | 0.00000 | 7 | (-0.33023+ 0.15093i); | 0.29024 |
| 8 | ( 0.24535+ 0.09745i); | 0.00000 | 8 | ( 0.26169+ 0.09211i); | 0.34682 |
| 9 | ( 0.24535+-0.09745i); | 0.00000 | 9 | ( 0.22763+-0.10719i); | -0.05492 |
| 10 | (-0.35425+-0.14888i); | 0.00000 | 10 | (-0.37829+-0.15073i); | -0.02133 |
| 11 | (-0.24535+ 0.09745i); | 0.00000 | 11 | (-0.22763+ 0.10719i); | 0.38846 |
| 12 | (-0.24535+-0.09745i); | 0.00000 | 12 | (-0.26169+-0.09211i); | -0.08743 |
| 13 | ( 0.00000+ 0.14944i); | 0.00000 | 13 | ( 0.02384+ 0.15134i); | 0.26040 |
| 14 | ( 0.11457+ 0.05397i); | 0.00000 | 14 | ( 0.14531+ 0.07004i); | 0.90858 |
| 15 | ( 0.00000+-0.14944i); | 0.00000 | 15 | (-0.02384+-0.15134i); | -0.02356 |
| 16 | ( 0.11457+-0.05397i); | 0.00000 | 16 | ( 0.08571+-0.05688i); | -0.10634 |
| 17 | (-0.11457+ 0.05397i); | 0.00000 | 17 | (-0.08571+ 0.05688i); | 1.01995 |
| 18 | (-0.11457+-0.05397i); | 0.00000 | 18 | (-0.14531+-0.07004i); | -0.07001 |

**APPLICABLE BLOCH WAVES**

| | | | | | |
|---|---|---|---|---|---|
| 1 | ( 0.73292+ 0.00000i); | 0.38051 | 1 | ( 0.73315+ 0.01586i); | 0.38066 |
| 3 | ( 0.59945+ 0.00000i); | 0.26390 | 3 | ( 0.60116+ 0.03088i); | 0.26517 |
| 5 | ( 0.35425+ 0.14888i); | 0.00000 | 5 | ( 0.37829+ 0.15073i); | 0.02119 |
| 7 | (-0.35425+ 0.14888i); | 0.00000 | 7 | (-0.33023+ 0.15093i); | 0.29024 |
| 8 | ( 0.24535+ 0.09745i); | 0.00000 | 8 | ( 0.26169+ 0.09211i); | 0.34682 |
| 11 | (-0.24535+ 0.09745i); | 0.00000 | 11 | (-0.22763+ 0.10719i); | 0.38846 |
| 13 | ( 0.00000+ 0.14944i); | 0.00000 | 13 | ( 0.02384+ 0.15134i); | 0.26040 |
| 14 | ( 0.11457+ 0.05397i); | 0.00000 | 14 | ( 0.14531+ 0.07004i); | 0.90858 |
| 17 | (-0.11457+ 0.05397i); | 0.00000 | 17 | (-0.08571+ 0.05688i); | 1.01995 |

[1]The beam direction is along the [010] zone axis and the incident angle is 6.5 mRad. The beam azimuth with respect to (100) plane is zero and the incident energy 100 keV.
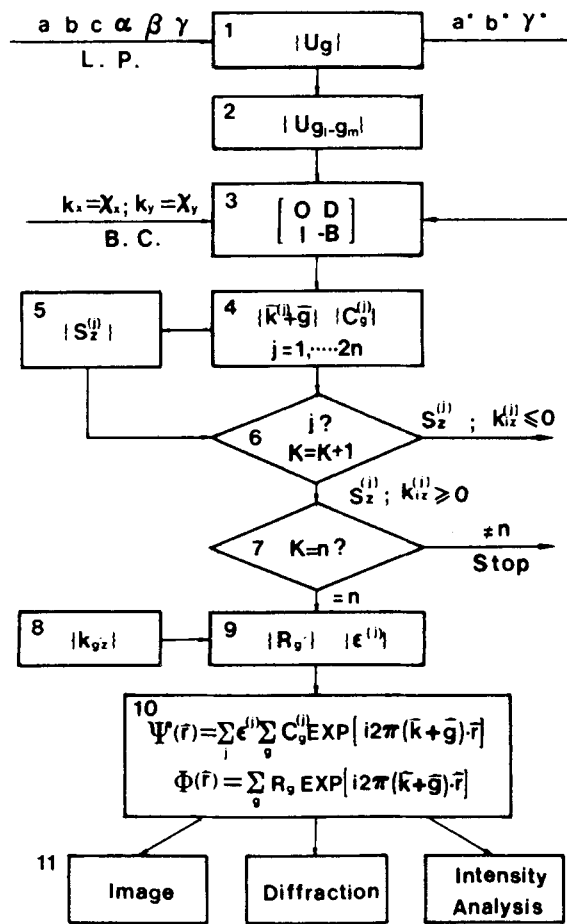
Fig. 1. An outline of the computer program for calculating the n-beam Bloch wave solution in the Bragg case.
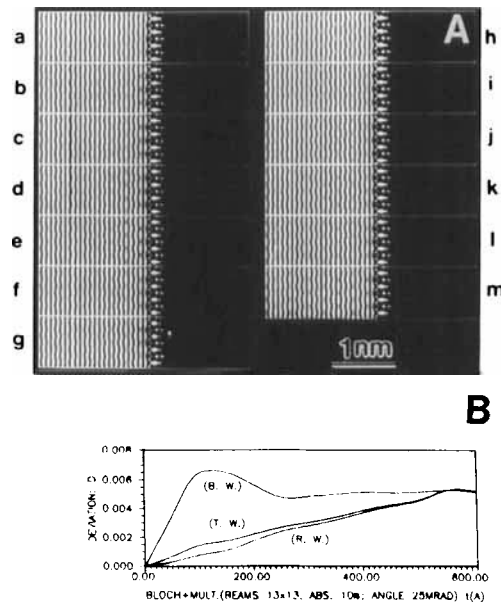


Fig. 2. A: Wave field outputs at different iteration thickness for 25 mRad incidence, 13 × 13 beam, absorption of 10%, and 100 keV incident energy, for Au (001) surface. B: Plots of the deviation parameters D versus thickness for current density outputs in A.
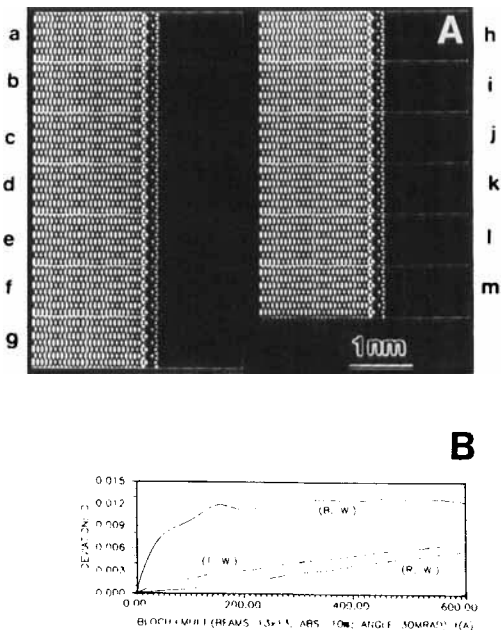


Fig. 3. Corresponding results under the same conditions as for Figure 2, except that the incident angle is 30 mRad.

the z axis is always the same as that of k vector. It should be noted that analyzing current flow in the Bragg case is not only significant for solving the boundary value problem but also useful for the understanding of physical insights of electron diffraction.

Once the excited Bloch states in a semi-infinite crystal in the Bragg case have been determined, the rest of the problem—boundary match in the Bragg case—is almost the same as that in the Laue case, for which readers can refer to the paper by Metherell (1975). Figure 1 shows an outline of a numerical development (Ma and Marks, 1989).

## BLOCH WAVE AND MULTISLICE COMBINED FOR REFLECTION (THE BMCR METHOD)

A problem of the Bloch wave method is that when a large number of beams are used, the computation speed is slow, and the method is also not readily available to simulate surface imperfections. Various alternative methods are therefore still necessary. In principle, all different methods must be consistent with each other under certain conditions, if they are correct. This suggests that it is possible to combine different methods

and to provide more powerful approaches. However, a precondition of combining different methods together is knowing their consistency conditions. The investigation of the consistency between the Bloch wave method and multislice can provide a clear-cut mutual proof of
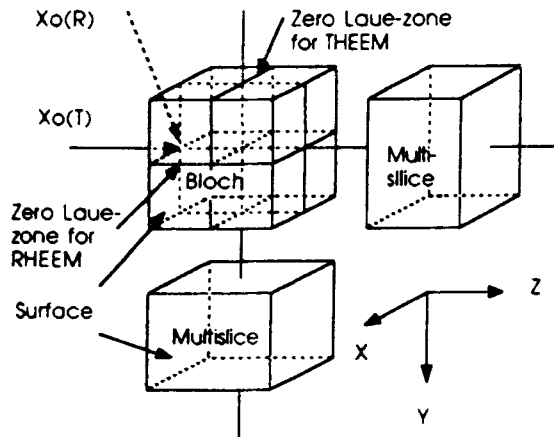
Fig. 4. The schematic diagram of the BMCR method. $X_o(R)$ denotes the incident wave vector in the reflection case and $X_o(T)$ denotes the incident wave vector in the transmission case. The zero Laue zones for the two cases are perpendicular to each other.
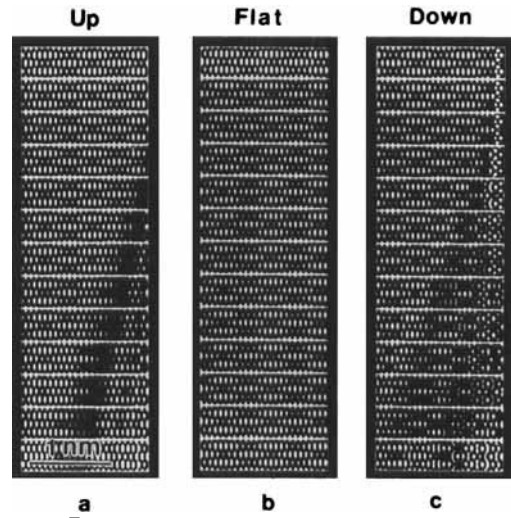


Fig. 5. Outputs of the wave fields in vacuum which include the Bragg reflected waves and the incident wave, from multislice iterations for the simulations of the surface with step-up (a), a flat surface (b), and the surface with step-down (c). The total thickness is 607.5 Å. The thickness difference between two nearest slices is 50 Å and the size of unit cell displayed is 4a × 1a, extending from surface (right side) into vacuum (left side). The step is introduced at t = 101.2 Å. The calculation conditions are the same as those for Figure 3.

the validity of the two methods and the combination of them and may also reveal more physical information about electron-crystal interactions, which will be discussed later.

## Consistency Between Bloch Waves and Their Multislicing in the Bragg Case

The Bloch wave method is a direct application of the Schrodinger equation to electron diffraction, while the multislice method was first developed using a physical optics approach. The analytical derivation of multislice formula from the Schrodinger equation was first given by Ishizuka and Uyeda (1977); see also Ma (1989) and Ma and Marks (1989). The Schrodinger equation in an integral form is given by:

$$\psi(r) = \exp(i2\pi k \cdot r) - (2m/4\pi h) \int G(r - r')V(r')\psi(r') \, dr' \quad (3)$$

where $\psi(r)$ is the wave function and $G(r)$ the Green's function. When the Green's function in the Schrodinger equation is written in the form of Rayleigh-Sommerfeld propagator (Gaskill, 1978), both the factoring of the wave function $(\psi(r) = \exp(i2\pi k \cdot r)\phi(r))$ and the Fresnel approximation are unnecessary. Moreover, the Fresnel approximation is incorrect for multislice calculations. Then the multislice formulation due to Cowley and Moodie (1957, 1959a, b) has the following forms:

$$\psi(q,z_{n+1}) = [\psi(q,z_n) \times P_g(q,z_{n+1} - z_n)] \cdot P_r(q,z_{n+1} - z_n)$$

or

$$\psi_{n+1}(q) = [\psi_n(q) \times P_g(q)] \cdot P_r(q,z_{n+1} - z_n) \quad (4)$$

where $q$ is a vector in the plane perpendicular to the beam direction along the z axis. For the Laue case, the two are consistent (Self et al., 1983). For the Bragg case, to test the consistency one can define a deviation parameter as (Ma and Marks, 1990a):
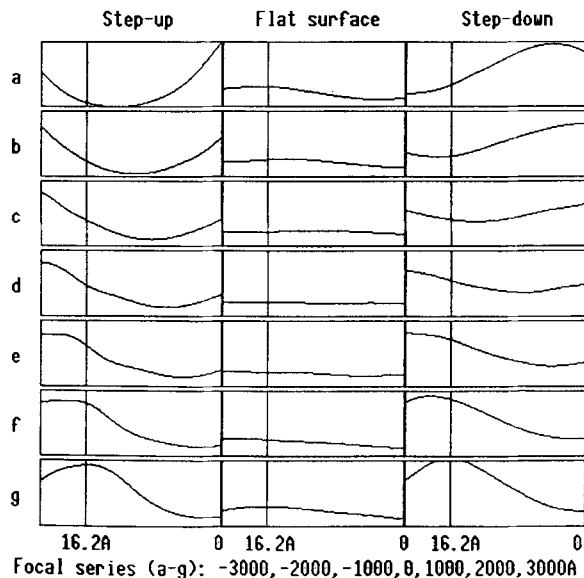


Fig. 6. Focal series of one dimensional imaging contrasts by using specular beam alone, crossing the wave disturbance caused by the steps in the second last slice (t = 556.8 Å) in Figure 5a–c. The defocus range is from −3,000 Å to 3,000 Å and defocus step is 1,000 Å.

$$D(t) = \Sigma_{x,y}[l_t(x,y) - l_0(x,y)]^2/\Sigma_{x,y}l_0(x,y)^2 \quad (5)$$

where $l_0$ denotes the intensity of the wave field calculated by the Bloch wave method which is an input wave field of multislice iteration and $l_t$ the intensity of the wave field output of multislice iteration at thickness t.

Note that the xy plane here is perpendicular to the incident beam direction and the slices are set normal to the surface. The magnitude of D(t) reflects the degree of the consistency between the two methods while the derivative of D(t), dD(t)/dt, indicates the convergence of the solution. The effects of various parameters on D(t), such as incidence angle, total calculated beam number, absorption, etc., have been studied (Ma and Marks, 1990a). Figures 2 and 3 are two calculated examples for fcc gold and the (001) surface. Figure 2A shows the wave intensity outputs at different thickness up to 607.5 Å for an incident angle of 25 mRad. Note that the incident energy for all calculations performed in this paper is 100 keV. The size of each slice is 8a × 2a (a denotes the magnitude of primitive unit cell vector of gold). The [010] zone is taken as the zero Laue zone and the surface normal is coincident with the z axis. The incident beam azimuth with respect to the yz plane is zero and the plane of the figure is parallel to the zero Laue zone. The number of beams calculated for the Bloch wave calculation is 13 × 13. Figure 2B shows the plots of D(t) versus thickness t, where R.W. denotes the reflected wave, B.W. the Bloch wave in crystal, and T.W. the total wave. Figure 3 shows the results for the same conditions as those for Figure 2, except that incident angle is 35 mRad. These results clearly indicate that the consistency on the [010] zone between the two methods in the Bragg case is well preserved (D(t) < 1%) and the solution converges (dD(t)/dt ≈ 0). It is important that the consistency is a confirmation of the current flow argument for the Bloch wave method.

However, it should be noted that all these results are obtained for the Au (001) surface and the conclusions here cannot be automatically extended to the surfaces with higher Miller indices. This will be discussed later.

## 2-D Dependence of the Bloch Wave and Picard Iteration-Like Character of Multislice Iterations in the Bragg Case

Equation 4 is a recursive solution of Equation 3, and if the electron wave function is known at the boundary, then the electron wave further down can be derived. If we have an electron wave field which is invariant along the z direction, Equation 3 has the following approximate form:

$$\psi(\mathbf{q},z) = [\psi(\mathbf{q},z) \times P_g(\mathbf{q},z - z_0)] \cdot P_r(\mathbf{q},z - z_0). \quad (6)$$

Note that this is an "equation," not a "solution." A true 2-D solution of Equation 6 can be solved by the Picard iteration:

$$\psi_{n+1}(\mathbf{q},z) = [\psi_n(\mathbf{q},z) \times Pg(\mathbf{q},z - z0)] \cdot Pr(\mathbf{q},z - z0) \quad (7)$$

$$\psi(\mathbf{q},z) = \lim_{n \to \infty} \psi_n(\mathbf{q},z). \quad (8)$$

Figures 2 and 3 indicate that the intensity of the wave field $l(\mathbf{r}) = \psi(\mathbf{r})\psi^*(\mathbf{r})$ in the Bragg case is independent of the distance along the beam direction when only the zero Laue zone is taken into account. In other words, in the Bragg case, the electron wave has the following form:
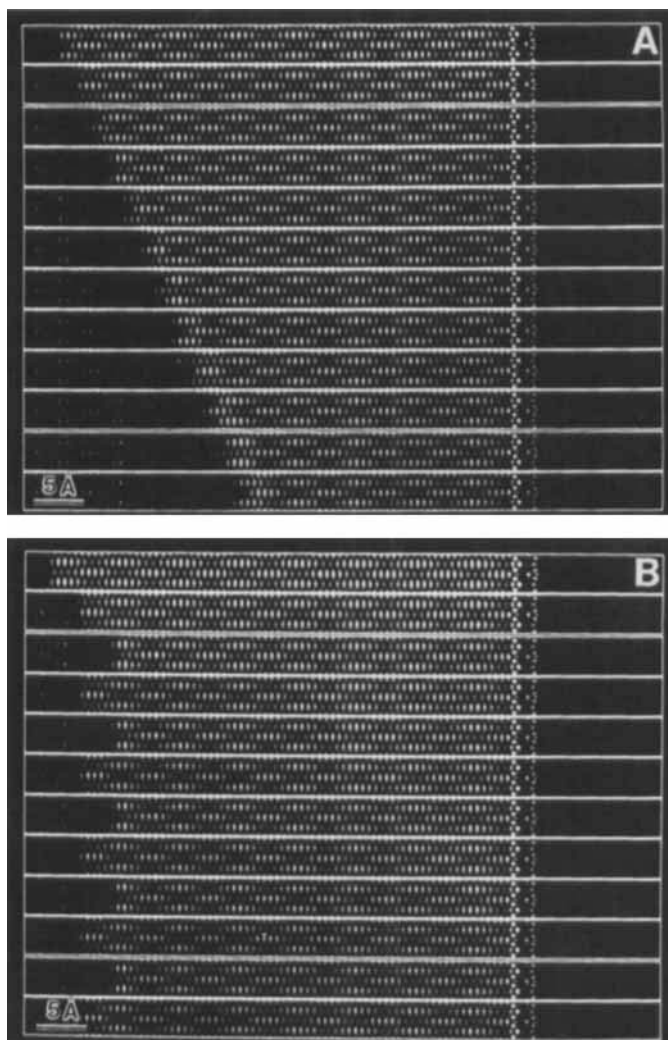


Fig. 7. **A:** Wave fields calculated by using the BMCR method without the edge patching method for Au (001) surface. The thickness difference between any two nearest slices is 50 Å. **B:** Wave fields calculated by using the BMCR method with the edge patching method for Au (001) surface. The thickness difference between any two nearest slices is 101.2 Å. Both A and B are calculated under the same conditions as those for Figure 3.

$$\psi(\mathbf{r}) = \psi(\mathbf{q},y) = \psi'(\mathbf{q})exp[i\phi(y)] \quad (9)$$

where the z axis is inward normal to the crystal surface and the incident beam direction is along the y axis. **q** is a real space vector in the plane perpendicular to the y axis. Equation 9 can also be proved analytically (Ma, 1990).

Substituting Equation 9 into Equation 7 and considering that the phase term $\phi(y)$ has a linear relation with y, $\phi(y) = cy$, we obtain:

$$\psi'(\mathbf{q})exp[i(n + 1)c\Delta y] = \{\psi'(\mathbf{q})exp[inc\Delta y] \times P_g(\mathbf{q},\Delta y)\} \cdot P_r(\mathbf{q},\Delta y). \quad (10)$$

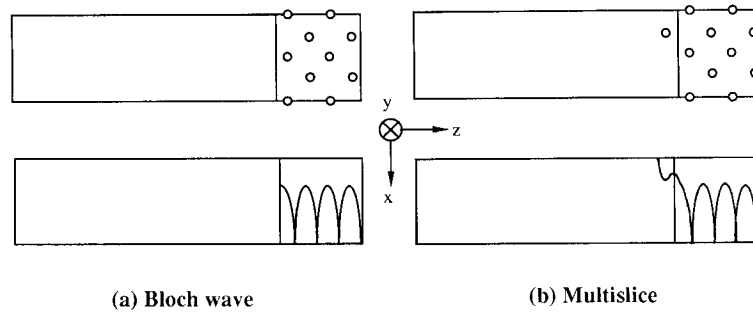(a) Bloch wave                                    (b) Multislice

Fig. 8. Unit cell set-up and potential profile for the simulation of surface reconstruction and adsorption. a: Unit cell with surface truncation for the Bloch wave calculation. b: Unit cell for multislice calculation. The unit size is 8a × 2a, a = 4.0497 Å.

Equation 10 shows two aspects of the multislice iteration in the Bragg case: on one hand, for $\psi'(q)$, each iteration is equivalent to a Picard iteration cycle; on the other hand, each iteration increments the phase by $\exp[ic\Delta y]$. In other words, the difference between the wave fields of any two slices is only a constant phase term: $\exp[imc\Delta y]$. This Picard iteration-like character of the multislice calculation shows that solving the wave field at a thickness deep enough by multislice is equivalent to solving the Schrodinger equation by a Picard iteration and if the iteration converges, it must converge to the stationary solution. Based on this feature, a new method which we call "Bloch wave and Multislice Combined for Reflection" (the BMCR method) was developed (Ma and Marks, 1990a, b). In this method, the Bloch wave solution for a free surface is taken as the input wave function for a multislice iteration, which is equivalent to the trial function of the Picard iteration for the stationary solution of an imperfect surface. Thus it reduced the edge effects of the multislice iteration down to the level which permits simulations of surface phenomena in a manageable and reliable manner and combines the advantages of the Bloch wave method and multislice approach together (stationary solution obtainable for the former and flexibility of surface imperfection simulation for the latter). Figure 4 shows a schematic diagram of the BMCR method.

As an example of the use of the BMCR method, Figure 5 shows the intensities of wave fields in vacuum for the surface with one step-up (a), a free surface (b), and the surface with one step-down (c). The size of each slice displayed is 8a × 1a. The right end of each slice is the position of the surface. For an atomic step-up, one layer of gold atoms is added to the surface and for an atomic step-down, the outermost layer of gold atoms is taken away from the surface. The total iteration thickness in each case is 607.5 Å, and the thickness difference between the two nearest slices is 50 Å. The incident angle is 30 mRad. There are two points which should be pointed out: 1) These simulations are performed under the stationary condition and the wave fields converge to the original stationary state after about 250 Å iterations during which the wave fields are disturbed by the steps. In other words, the transi-

tion range of 200–250 Å begins and ends with a stationary state. 2) Wave field disturbances caused by surface steps and carried by the Bragg reflected waves are moving away from the crystal surface, which means that the information about the steps exists in each reflected beam, and the image formed from any reflected beam will show the contrast of the steps.

To simulate REM operation in an electron microscope, the specular beam was used for imaging and the optical axis tilted to be coincident with the specular beam. One dimensional images for the last slices in Figure 5a–c are shown in Figure 6. They are the plots of wave intensities versus the distance extending from the surface into vacuum (0–6 × 4.0497 Å, from right to left). Each column is a focal series from −3,000 Å to 3,000 Å. A contrast reversal with defocus is quite clearly demonstrated. The contrast of a free surface (central column) is due to numerical error. To quantitatively estimate the errors, the contrast level of each picture is calculated as CONTRAST = SD/MEAN, where SD is the standard deviation and MEAN is the mean level of the picture. The value of the CONTRAST is averaged over each focal series in Figure 6. We have three contrast levels for three different surfaces: 0.58 (step-up), 0.13 (flat surface), and 0.31 (step-down). The error is from 22% to 40%. Note that the results suggest that the contrast level of a step-up is generally higher than that of a step-down.

## EDGE PATCHING METHOD
### The BMCR Method With Edge Patching

The BMCR method provides a more favorable condition for the simulation of HEER. However, it only reduces the edge effects in multislice instead of eliminating them. Later, it will be shown that even this advantage of the BMCR method is limited because the BWO solution can be far from the true stationary solution when the zero Laue zone is [1$\bar{1}$0] other than [010].

To obtain an infinitely convergent stationary solution not limited by iteration thickness for an arbitrary crystal surface, one must solve the problem of the inward moving edge. Because there is only a constant phase difference $\exp[imc\Delta y]$ between any two slices for the multislice iterations in the Bragg case, as indicated

by Equation 10, the deteriorated edge can always be replaced by the edge cut from the original input wave field as long as it is multiplied by a proper phase $\exp[imc\Delta y]$; c can be calculated either analytically or numerically. This is called "patching" (Ma, 1990). It is not necessary to repair the deteriorated edge for each iteration because the moving edge seriously deteriorates the solution only after a certain number of iterations and then the computation time will not increase significantly because of the "repairing." The rate of deterioration of the edge primarily depends upon three parameters: incidence energy ($E_0$), incidence angle ($\theta_0$), and slice thickness ($\Delta z$), and the frequency of repairing can be set self-adjustable in the program.

Figure 7 shows a comparison between the wave field calculated with and without the edge patching using the BMCR method. The calculation conditions are the same as those for Figure 3, except that the displayed slice size here is 16a × 1a instead of 8a × 2a. The thickness between any two nearest slices in Figure 7A is 50.6 Å, while it is 101.2 Å in Figure 7B, i.e., the total thickness calculated in B is twice as large as that in A: 1,113.2 Å. The value in Figure 7A was calculated using the BMCR method without edge patching, while that in Figure 7B was calculated using the BMCR method with the edge patching. The patched edge area in B is 1/3 of the area of the vacuum wave along the z axis. The continuity between the patched edge area and nonpatched area in B is clearly demonstrated and the deteriorated edge has disappeared. In other words, a convergent true stationary solution not limited by iteration thickness has been obtained. However, this is still not a real proof of the infinity of the convergence, because here, the Bloch wave solution as an input wave field of multislice iterations is already close to the true stationary solution. If the Bloch wave solution is far from the true stationary solution, there will be discontinuity between the patched edge area and non-patched area of the vacuum waves, for example, the true stationary solution for a reconstructed surface will be quite different from the Bloch wave solution of a corresponding non-reconstructed free surface.

To examine this, calculations for a surface reconstruction and adsorption in RHEED were performed. Figure 8 shows the unit cell for the Bloch wave calculation and the multislice iterations in Equation 6, which includes surface reconstruction or adsorption. The system used is fcc gold. The treatment of absorption is the same as that for Figures 2 and 3. For the 2 × 1 reconstruction or adsorption, the vertical dimension of the unit cell needs to be two times larger than the primitive vector, so the size of the two unit cells is 8a × 2a. The surface is set at (3/4,0) and the other calculation conditions are the same as those for Figures 2 and 3.

For the 2 × 1 gold surface reconstruction, one gold atom is placed on the site indicated in Figure 8b for each of four slices with no relaxation. For a 2 × 1 chemisorbed oxygen surface, the gold atom was replaced by an oxygen atom. Figure 10 shows output of wave intensities from multislice iterations for the 2 × 1 gold reconstruction in A and the 2 × 1 oxygen adsorption in B. The series of output slice numbers are: 1,
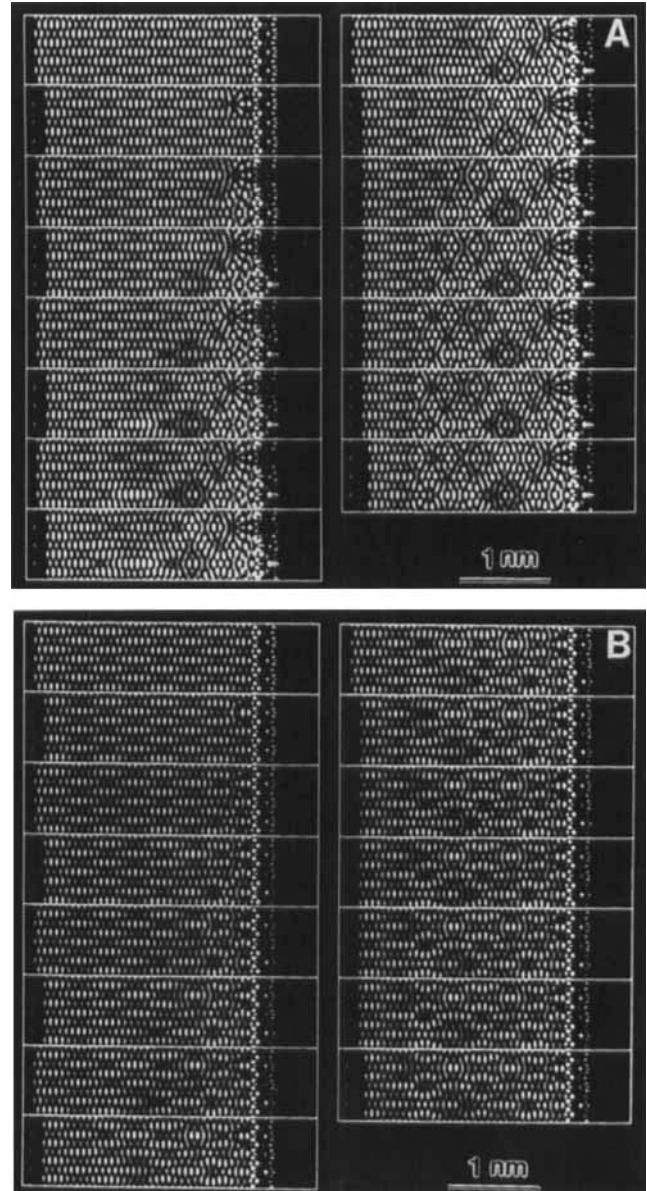


Fig. 9. A: Wave fields calculated for the 2 × 1 Au (001) surface using the BMCR method with the edge patching method. B: Wave fields calculated for the 2 × 1 oxygen adsorption on an Au (001) surface using the BMCR method with the edge patching method. The series of output slice numbers are: 1, 100, 200, 300, 400, 500, 600, 700, 800, 900, 1,000, 1,100, 1,300, 1,500, 1,700, 2,050. The calculation conditions are the same as those for Figure 3.

100, 200, 300, 400, 500, 600, 700, 800, 900, 1,100, 1,300, 1,500, 1,700, 2,050. The iteration thickness is up to 2,075.5 Å, which is much thicker than what was previously possible. The last four slices in Figure 9A or B show that the stationary wave field for a surface with either reconstruction or adsorption has been reached in the non-patched area. The wave field in the patched areas is quite different from the stationary wave field in the non-patched area on the right because it is cut
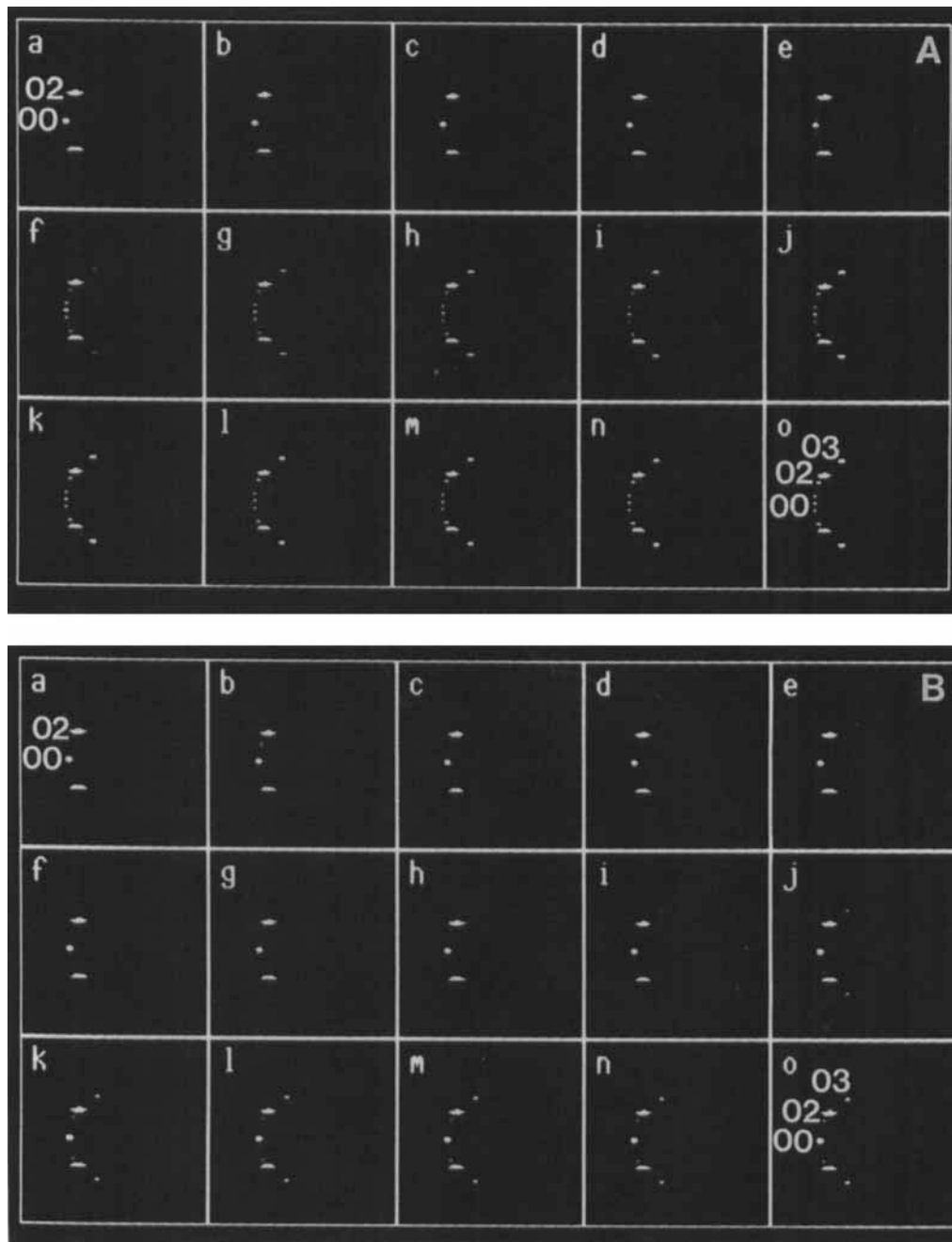
Fig. 10.   A: RHEED patterns corresponding to Figure 9A. B: RHEED patterns corresponding to Figure 9B.

from the solution of a free surface. Nevertheless, this inconsistency does not affect the stationary solution of an imperfect surface in the non-patched area. This can be further demonstrated in reciprocal space. Figure 10A and B show the RHEED patterns corresponding to Figure 9A and B. They are Fourier transforms of the vacuum waves excluding the patched areas in the slices in Figure 9A and B. It should be noted that the stationary character of these solutions is apparent. This phenomenon can be explained as the following:

The vacuum wave in each slice is the superposition of two parts, the incident wave and the Bragg reflected waves. The Bragg reflected wave front always moves away from the crystal surface while the incident wave front moves towards the crystal surface, which is the major source of the edge effects. When the edge patching is carried out, both of them are multiplied by a constant phase term. In the case of poor trial function, the Bragg reflected wave components may be far from the true solution, but the incident plane wave is always

the same. Because the wave front of the Bragg reflected waves always moves away from the surface, it does not matter if they are close to the true solution. What is important is the continuity of the incident plane wave field for each patching and iteration. This is the reason why the infinitely convergent true stationary solution is reached with a "bad" input trial function.

### The Edge Patching Method in Multislice-Only Mode (the EPMO Method)

The above argument implies that a plane wave should also be usable as a trial wave, since only the incident plane wave component in the patched area is significant to the continuity of multislice iterations. In other words, an independent computation method called "the Edge Patching method in Multislice-Only mode" (the EPMO method) can be used.

When the computation program is shifted to multislice-only and reflection mode, the results shown in Figures 11 and 12 are obtained. They correspond to Figures 9 and 10. All of the calculation conditions are the same as those for Figures 9 and 10, except for the input trial wave function which is now tilted plane wave (30 mRad) instead of the BWO solution of a perfect surface. The results shown in Figures 11 and 12 are clearly consistent with those shown in Figures 9 and 10. However, there is now only one plane wave component left in the patched area which acts like an "infinite plane wave source." This simulates the real condition of an electron microscope or a RHEED camera which usually has a beam size of several tens of nanometers. The results show that an incident beam with this size can be modeled as an infinite plane wave not only in the Laue case but also in the Bragg case. The first ones of RHEED patterns in Figure 12A and B do not show any diffraction spot because there is only one incident wave component masked to allow for a clearer presentation of the Bragg spots. In real experiments, the incident beam is cut off by the crystal edge.

### Analysis of the Higher Order Laue Zone Using the EPMO Method

For the EPMO method, only the plane wave component in the patched area is significant to the multislice calculation and the function of the patched edge area is only to provide an infinite plane wave source. It does not require the wave fields inside and outside the crystal to be 2-D dependent and the multislice iterations to be Picard iteration-like. An analysis of higher order Laue zone requires sampling of the crystal potential along the beam direction, and the phase gratings for each slice are no longer identical to each other. Here, each iteration is no longer Picard iteration-like and the wave field is no longer 2-D dependent in a distance of one unit cell in the incident beam direction. However, for any two slices separated by a distance of an integral number of unit cells in the incident beam direction, the above two arguments are still valid. As matter of fact, the variation of the wave fields in a distance of one unit cell in the incident beam direction for HEER is small, because the effects of the higher order Laue zones are weak. Figure 13A is the result calculated for the Au
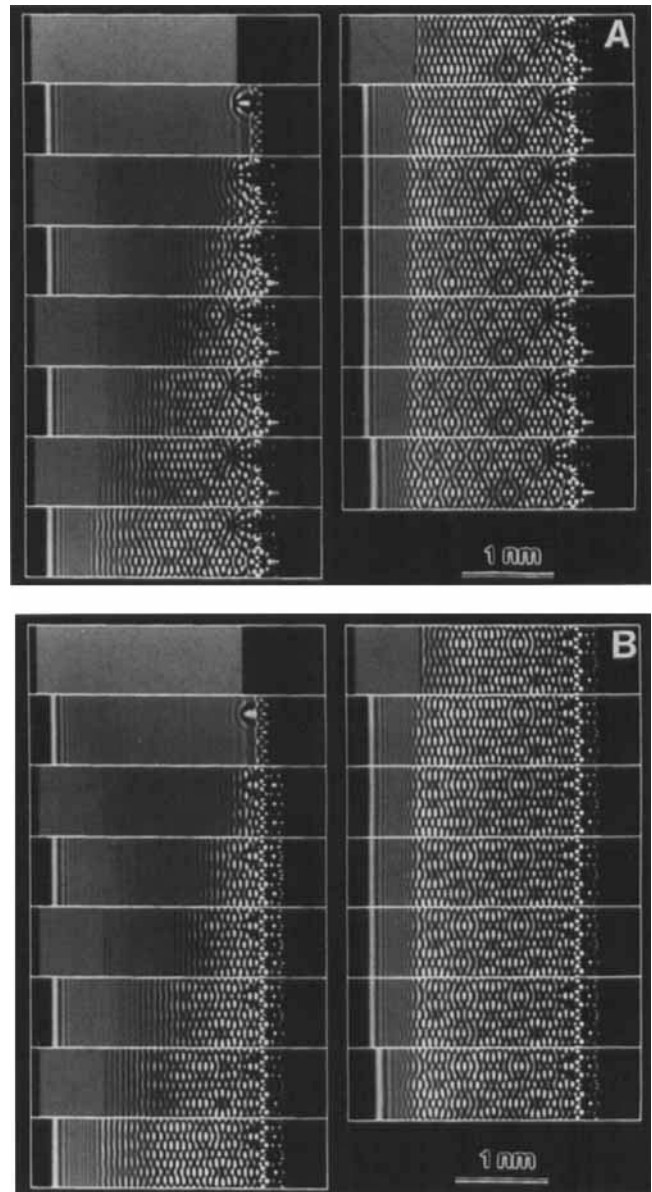


Fig. 11. **A, B:** Wave fields calculated for the same system and conditions as those for Figure 9, except that the EPMO method is used.

(110) surface using the EPMO method. The incident angle is 30 mRad and the absorption is the same as that for Figures 2 and 3. The crystal potential is now sampled along the [1$\bar{1}$0] zone axis. The sampling rate is 2.78 pts/Å, i.e., eight slices for each unit cell along the [$\bar{1}$10] direction (2.88 Å). The series of output slice numbers is: 1, 800, 1,000, 2,000, 3,000, 4,000, 5,000, 6,000, 7,000, 8,000. The iteration thickness is up to 2,884.0 Å. The sampling was done by applying a solid Gaussian distribution, $G(x) = (c/\sqrt{2}\pi\sigma)\exp(-x^2/2\sigma^2)$, onto the occupancy parameters of atoms in each phase grating; c is a constant for normalizing the total occupancy of
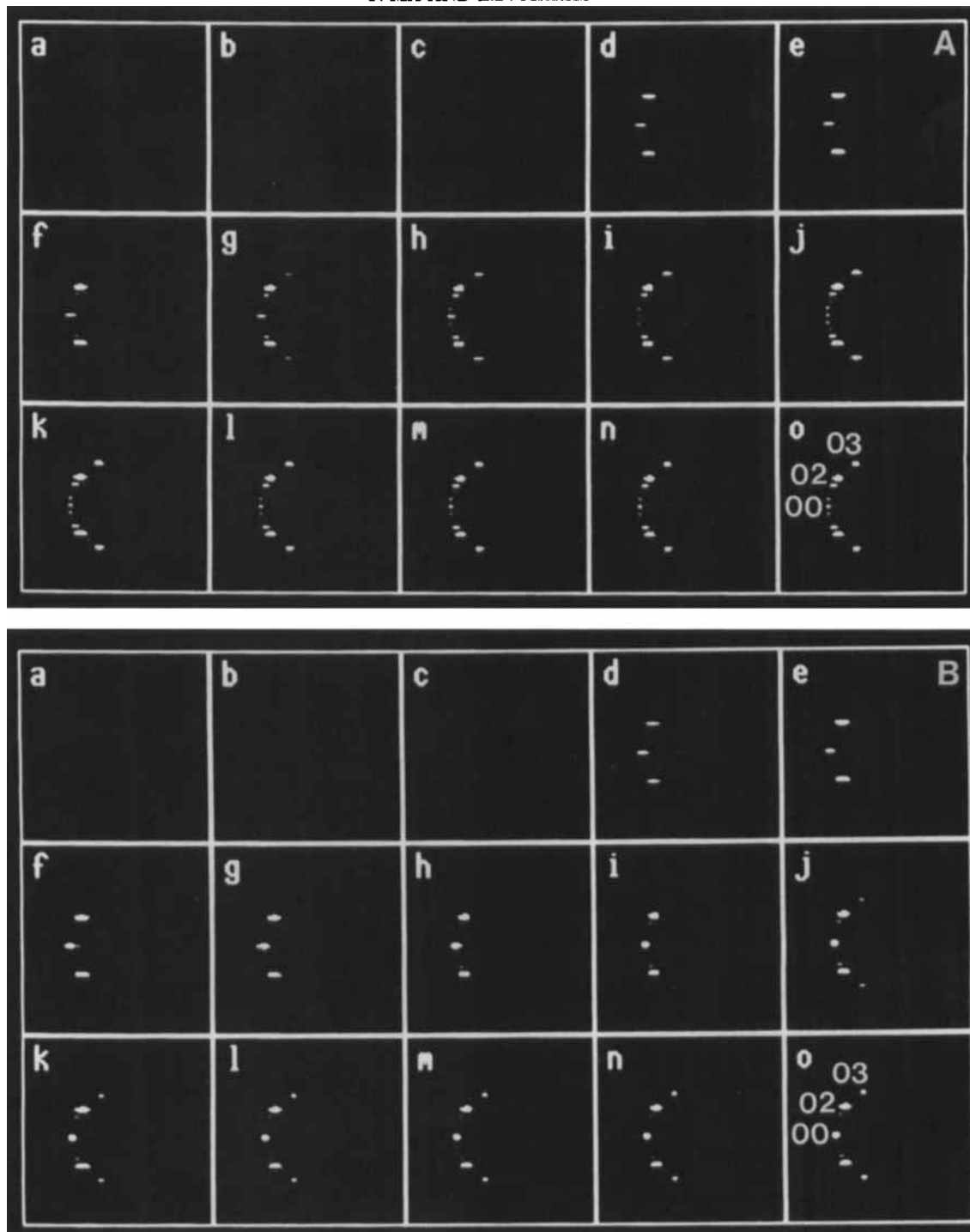
Fig. 12.   **A, B:** RHEED patterns corresponding to Figure 11.

each atom to 1; s is set to 0.125. The last three slices in Figure 13 show the stationary solutions and they are invariant with the thickness.

Figure 13B shows the RHEED patterns including the first and second order Laue zone. They are the Fourier transforms of the vacuum waves excluding the patched edge area of the last slices in Figure 13A. For showing the weak spots of the first and second order Laue zone, the incident spot and the Bragg reflected spots of the zero order Laue zone have been saturated (Fig. 13Ba). These spots become streaky due to numerical errors. Especially, the incident spot turns into a

Fig. 13. A: Wave fields calculated for Au (110) surface using the EPMO method. The zero Laue zone is [1Ī0] and the crystal potential is sampled along the [Ī10] direction. Other calculation conditions are the same as those for Figure 3. B: RHEED patterns corresponding to A.

long bright line. They should not be considered as real effects of HEER. For a clear presentation of different Laue zones, the incident spot is excluded and the zero Laue zone is shown in Figure 13Bb and the first and the second Laue zones are shown in Figure 13Bc. The symmetry of the zero order Laue zone is well preserved. The asymmetry of the first and second Laue zones is quite visible. This is due to the existence of numerical errors after 8,000 iterations. The intensities of spots in the second Laue zone are so low that they are more easily affected by numerical errors. The sampling rate along the [Ī10] direction, 2.78 pts/Å, is much lower than the sampling rate in the plane perpendicular to the incident beam (10–15 pts/Å). However, the results

clearly demonstrate the capability of the EPMO method for surface investigation using the information of higher order Laue zones in HEER.

## LIMITATION OF THE BWO SOLUTION
### Failure of the BWO Solution for Au (110) Surface

For a long time, the effects of surface potential and surface topmost structure on HEER have not been studied systematically due to the lack of a reliable method to simulate HEER for an arbitrary surface. This problem is crucial to the Bloch wave method because it is basically a method for bulk materials and is not sensitive to the structure of boundary. If the effects are important, the BWO solution for HEER will be
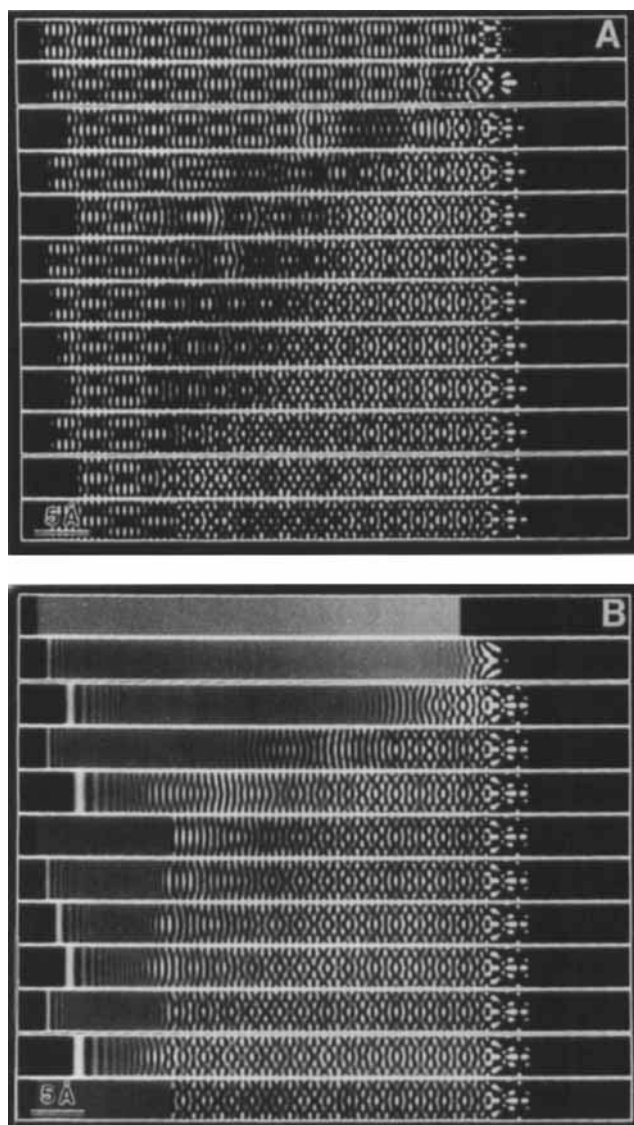
Fig. 14. A: Wave fields calculated by using the BMCR method with the edge patching method for Au (110) surface. B: Wave fields calculated by using the EPMO method for Au (110) surface. The series of slice numbers for both A and B are: 1, 100, 300, 600, 900, 1,000, 1,100, 1,200, 1,300, 1,500, 1,700, 2,050. Both A and B are calculated under the same conditions as those for Figure 13, except that the crystal potential is not sampled along the [1̄10] zone axis.

questioned. Comparison of the BWO solution and multislice in the Bragg case for Au (001) surface as discussed before (Ma and Marks, 1990a) showed that the surface potential and the surface truncation do not affect the consistency and quality of the BWO solution significantly. However, further studies show that this conclusion cannot be extended to the case of a surface with higher Miller indices as one might expect.

Figure 14A and B are results calculated for the Au (110) surface using the BMCR method and EPMO method, respectively. The size of each slice in both A

and B is $10\sqrt{2}a \times 1a$. The surface is at (3/4,0) and the sampling array is $1,024 \times 64$. The coordination and beam geometry are as the following: the [1̄10] zone is taken as the zero Laue zone; the z axis [1̄10] goes from the left side to the right side pointing toward the inside crystal, the y axis [1̄10] is parallel to the inward normal to the page, and the x axis is along the [001] direction. The incident beam is along the y axis and the beam azimuth with respect to the yz plane is zero; 2,050 iterations have been calculated and the total thickness of each calculation is up to 2,956.1 Å. The series of output slice numbers are: 1, 100, 300, 600, 900, 1,000, 1,100, 1,200, 1,300, 1,500, 1,700, 2,050. The two solutions are perceivably close to each other, which means that both the BMCR method and EPMO method can provide well converged solutions. The most important feature of Figure 14A is that the severe deviation of the BWO solution from the stationary solution for the Au (110) surface has been revealed. In other words, the BWO solution for the Au (110) surface is no longer a good trial function of multislice iterations.

Figure 15A and B show the RHEED patterns corresponding to Figure 14A and B, respectively. They are the Fourier transform of the vacuum waves excluding the patched edge area in each slice in Figure 14A and B. Figure 15 indicates that there are significant differences between the first pattern (the BWO solution) and the last pattern in A (the BMCR solution) or B (the EMPO solution). For the diffraction pattern of the BWO solution, there are three Bragg reflected spots: one specular spot and two (02) spots. The (01) and (03) spots are missing. With the process of iterations, the (01) and (03) spots in Figure 15A gradually emerge and the intensities of two (02) spots finally reduce to near zero, while Figure 15B only shows the (01) and (03) spots.

## A Qualitative Explanation of the Failure

The RHEED patterns shown in Figure 15 give a clear and important qualitative explanation of the failure of the BWO solution for Au (110) surface. The BWO solution is basically a solution for a bulk crystal. As far as the bulk material is concerned, the distance between two adjacent atomic planes parallel to the zone axis and surface normal is a/2 for both the [010] zone and the [1̄10] (Fig. 16). Therefore, the singular Bragg reflection spots (01) and (03) corresponding to the interplanar distance a should be extinct, as indicated by the BWO solution in Figure 16A. Nevertheless, HEER is primarily a surface phenomenon and sensitive to the structure of the top atomic layer. The materials joining the diffraction process are limited to several top atomic planes. As indicated by Figure 16B, for the Au (110) surface, the atomic distance of the topmost layer is a instead of a/2 for the Au (001) surface. This is the major reason for sharp intensity decline of the (02) spots and strong emergence of the (01) and (03) spots in the RHEED patterns of the EPMO and BMCR solutions. This argument can be further verified by Figure 17 which is the result calculated by using the EPMO method under the same conditions as those for Figure 14A, except that the absorption is set as 0%, i.e., no
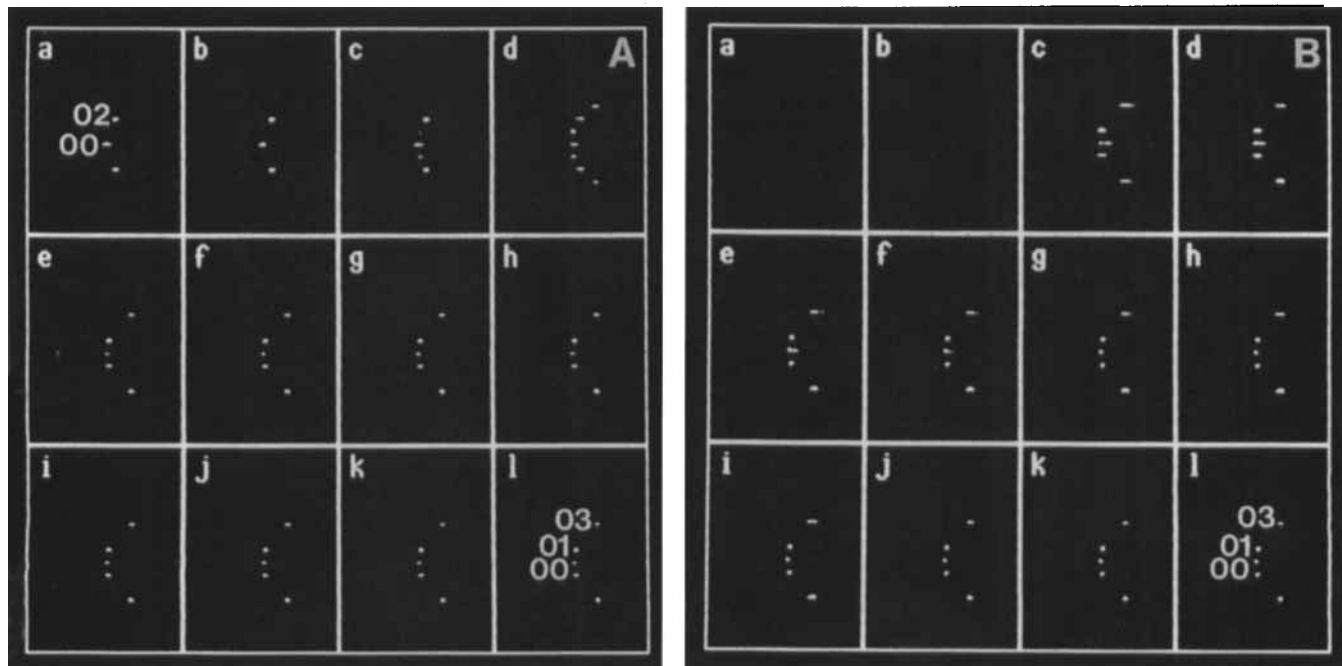
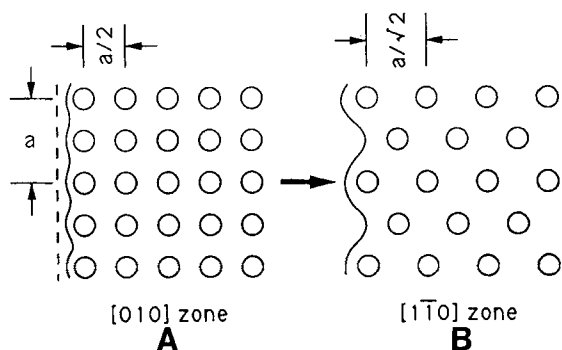Fig. 15.   A, B: RHEED patterns corresponding to Figure 14A and B.



Fig. 16.   Schematic diagram of atomic arrangement of Au in the [010] A and [1$\bar{1}$0] B zones.

imaginary potential. This allows the atoms deep in the crystal to join the diffraction process. Then the diffraction process becomes the mixture of surface phenomena and bulk phenomenon. The patterns of the vacuum waves in the last four slices in Figure 17A are perceivably different from those in Figure 14A. Figure 17B shows the RHEED pattern of the vacuum wave excluding the patching edge area in each slice in B. The re-emergence of the (0$\bar{2}$) spots in Figure 17B is due to the bulk diffraction and the spots (0$\bar{1}$) and (0$\bar{3}$) are still there, which represent the diffraction process of the top atomic layers.

For the [010] zone, the bulk process and surface process have the same effects on RHEED pattern, as in-

dicated in Figure 16A. Then the BWO solution becomes close to the true stationary solution obtained by the BMCR method or the EPMO method. Here, we can have a straightforward deduction: the intensities of the Bragg spots in the RHEED patterns are generally penetration depth related, except for a simple surface like the (001) surface. The deeper the incidence electrons penetrate into the crystal, the more bulk effects there will be in the RHEED patterns.

### A Cure of the BWO Solution for the Surfaces With Higher Miller Indices

In terms of the theory of Bloch waves, the source of the error can only be the boundary match. As shown in Figure 16, the flat surface match for the (001) surface is a good approximation, but it is poor for the (110) surface. The flat surface match actually can be replaced by a periodic non-flat surface match, which is numerically feasible. Here, we give an analytical derivation of it. For the flat surface match, we have the following two equations:

$$\Phi(\tau,z) = \Psi(\tau,z) \tag{11}$$

$$\partial\Phi(\tau,z)/\partial z = \partial\Psi(\tau,z)/\partial z|\tau = (x,y), z = 0 \tag{12}$$

where $\Phi$ is the wave function of the wave outside crystal, $\Psi$ the wave function of the wave inside crystal, the surface is set in the xy plane, and the surface normal is parallel to the z axis. For a periodic non-flat surface match, we have:
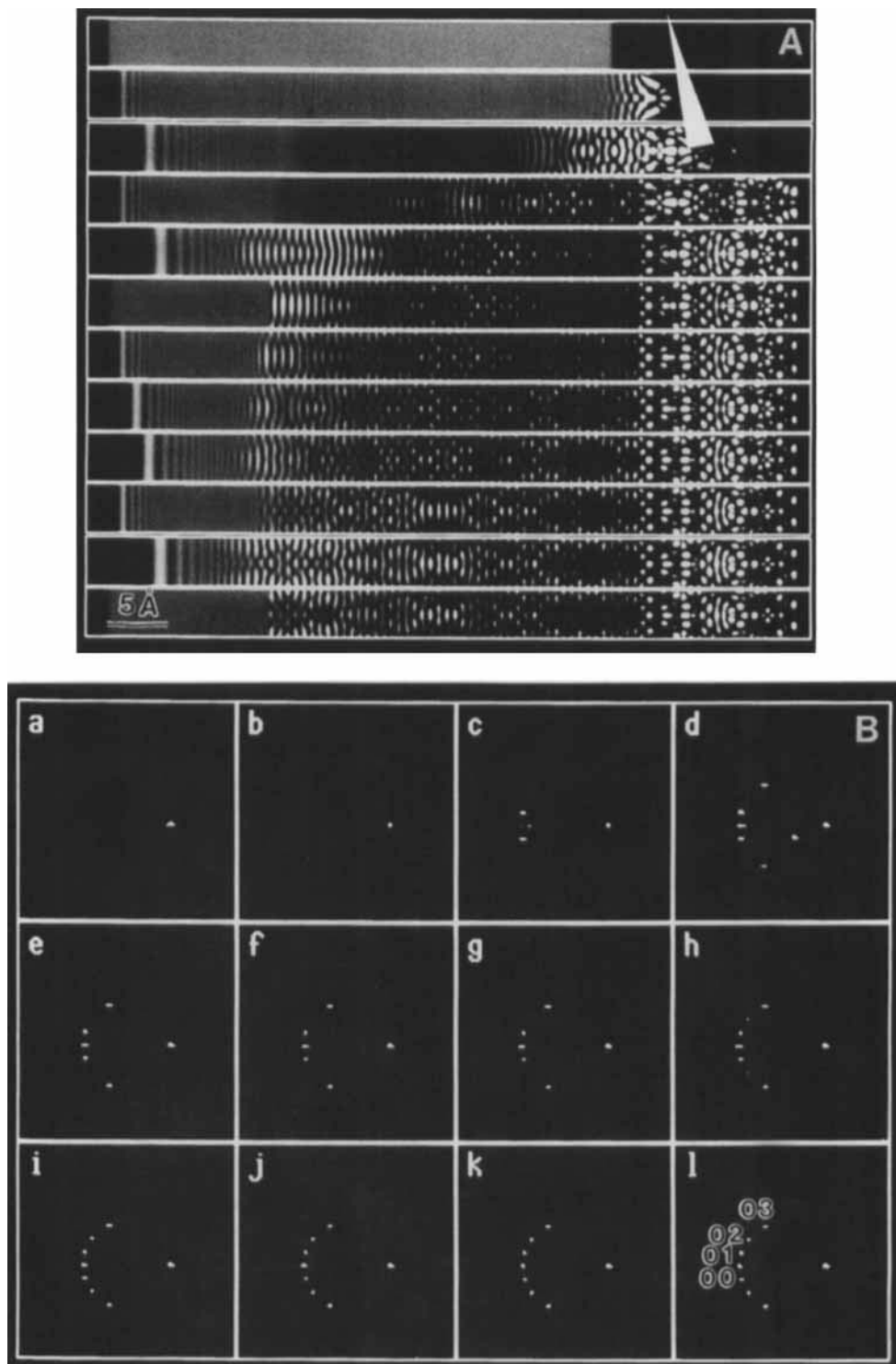
Fig. 17.   A: Wave fields calculated by using the EPMO method under the same conditions as those for Figure 14A, except that the absorption is set as 0%. B: RHEED patterns corresponding to A.

$$\Phi(\tau,z) = \Psi(\tau,z) \tag{13}$$

$$\partial\Phi(\tau,z)/\partial z = \partial\Psi(\tau,z)/\partial z|\tau = (x,y), \; z = f(x,y) \tag{14}$$

where f(x,y) is a 2-D periodic function and its approximate form can be easily derived. Both Equations 13 and 14 can be expanded into the form of Fourier series:

$$\Sigma_{g'}(\delta_{g'o'} + R_{g'})\exp[i2\pi(k_{ot'} + g_t')\cdot\tau]$$
$$\exp[i2\pi(k_{oz'} + g_{z'})f(x,y)]$$
$$= \Sigma_j\epsilon^{(j)}\Sigma_g C_g^{(j)} \exp[i2\pi(k_{ot} + g_t)\cdot\tau]$$
$$\exp[i2\pi(k_{oz}^{(j)} + g_z)f(x,y)] \tag{15}$$

$$\Sigma_{g'}(k_{oz'} + g_z')(\delta_{g'o'} + R_{g'})$$
$$\exp[i2\pi(k_{ot'} + g_t')\cdot\tau]\exp[i2\pi(k_{oz} + g_z')f(x,y)]$$
$$= \Sigma_j\epsilon^{(j)}\Sigma_g(k_z^{(j)} + g_z)C_g^{(j)}\exp[i2\pi(k_{ot} + g_t)\cdot\tau]$$
$$\exp[i2\pi(k_{oz}^{(j)} + g_z)f(x,y)] \tag{16}$$

where $C_g^{(j)}$ is the coefficient of a plane wave component g of a Bloch wave j, $\epsilon^{(j)}$ excitation coefficient of the Bloch wave j, $R_{g'}$ the coefficient of a Bragg reflected wave g', and δ is Kroeniger's delta function.

The exponential terms with f(x,y) in Equations 15 and 16 can be further expanded into Fourier series as the following, since f(x,y) is a 2-D periodic function:

$$\exp[i2\pi(k_{oz'} + g_z')f(x,y)] =$$
$$\Sigma_{h'}\alpha_{g',h'}\exp[i2\pi(k_{ot'} + h_t')\cdot\tau] \tag{17}$$

$$\exp[i2\pi(k_{oz}^{(j)} + g_z)f(x,y)] =$$
$$\Sigma_h\beta_{g,h}^{(j)}\exp[i2\pi(k_{ot} + g_t)\cdot\tau] \tag{18}$$

where $\alpha_{g',h'}$ and $\beta_{g,h}^{(j)}$ can be calculated numerically. Substituting Equations 17 and 18 into Equations 15 and 16 and letting g' + h' = l' and g + h = l, we obtain:

$$k_{ot'} = k_{ot} \tag{19}$$

$$\xi_l = \Sigma_j\epsilon^{(j)}A_l^{(j)} \tag{20}$$

$$k_{oz'}\xi_l = \Sigma_j\epsilon^{(j)}B_l^{(j)} \tag{21}$$

where

$$\xi_l = \Sigma_{g'}(\delta_{g'o'} + R_{g'})\alpha_{g',l-g'} \tag{22}$$

$$k_{oz'}\xi_l \approx \Sigma_{g'}(k_{oz'} + g_{z'})(\delta_{g'o'} + R_{g'})\alpha_{g',l-g'} \tag{23}$$

$$A_l^{(j)} = \Sigma_g C_g^{(j)}\beta_{g,l-g}^{(j)} \tag{24}$$

$$B_l^{(j)} = \Sigma_g(k_z^{(j)} + g_z)C_g^{(j)}\beta_{g,l-g}^{(j)}. \tag{25}$$

$\epsilon^{(j)}$ and $\xi_l$ can be solved by Equations 20 and 21 and then $R_{g'}$ can be solved by Equation 22. Although the process as shown here is more tedious than that for the flat surface match, the 2-D periodic surface match in principle can be done. In other words, the BWO method can be applied for not only an ideal flat surface model, but also all kinds of periodic non-flat surface models.

## CONCLUSION

The argument of current flow appears to clear the confusion around evanescent waves in the "band gap." The consistency between the BWO solution and its multislicing for an Au (001) surface has verified the validity of the argument of the current flow. The application of the BMCR method to the problems of surface steps and surface reconstruction or adsorption has demonstrated the usefulness of the method. The two most important characters of HEER—2-D dependence of the wave fields and the Picard iteration-like character of the multislice calculations in the Bragg case—have led to the emergence of an edge patching method or EPMO method. An infinitely convergent true stationary solution for any arbitrary surface for HEER has been obtained using the new method.

The failure of the BWO solution for surfaces with higher Miller indices is troublesome, but the EPMO method is simple and accurate enough to be a quantitative method for HEER analysis on any kind of surfaces, as far as the zero Laue zone is concerned. The method has also shown its capability for dynamical analysis of the higher order Laue zones in HEER.

However, so far the problems in HEER which can be explained by dynamical approaches including the BMCR and EPMO methods are still limited. It is obvious that any RHEED pattern obtained in experiments is far more complicated and informative than any one simulated. The theory discussed here is only elastic and a lot of surface phenomena such as surface plasmons, thermal diffuse scattering, strain fields, etc., cannot be easily taken into account in the theory. As far as the application is concerned, the reliability of a quantitative analysis using the BMCR and EPMO methods needs to be further tested in the application to real problems. For example, the quantitative analysis of disordered steps is not really as yet practical. The explanation and suggested cure of the failure of the BWO solution for surfaces with higher Miller indices still need to be further examined. There are still two basic experimental phenomena in HEER which remain unanswered, or incompletely answered, and merit further study:

1. The source of two dimensional diffraction patterns observed in RHEED experiments. So far, all simulated RHEED patterns are semi-circular type and consistent with most of those taken by using RHEED cameras. Some of RHEED patterns taken from surfaces such as Au (111) and Pt (111) in a microscope show a clear two dimensional feature, which seems contradictory to the law of momentum conservation according to the elastic theory.

2. The true source of "electron surface resonance." All calculations by the BWO, BMCR, and EPMO so far do not show as strong intensity enhancements around the resonance conditions as experiments do. Before one can give a quantitative analysis on the "electron surface resonance spectrum," the term "electron surface resonance" still means more as an experimental fact rather than a physical concept.

## REFERENCES

Bertrand, O., Floquet, N., and Jacquot, D. (1985) The crystallographic shear planes of the non-stoichiometric molybdenum oxides as revealed by RHEED investigation from the $Mo_{18}O_{52}$ (100) surface. Surface Sci., 164:305–319.

Bethe, H. (1928) Theorie der Beugung von Elektronen an Kristallen. Ann. Phys., 87:55–129.

Borries, B. v. (1940) Sublichtmikroskopische Auflosungenbei der Abbildund von Obserflachen im Ubermikroskop. Z. Phys., 116:370–863.

Cohen, P.I., Pukite, P.R., Van Hove, J.M., and Lent, C.S. (1986) Reflection high energy electron diffraction studies of epitaxial growth on semiconductor surface. J. Vac. Sci. Technol., A4(3):1251–1258.

Colella, R. (1972) N-beam dynamical diffraction of high-energy electrons at glancing incidence, general theory and computation methods. Acta Crystallogr., A28:11–15.

Colella, R., and Menadue, J.F. (1972) Comparison of experimental and n-beam calculated intensities for glancing incidence high-energy electron diffraction. Acta Crystallogr., A28:16–22.

Cowley, J.M., and Hojlund Nielsen, P.E. (1975) Magnification variations in reflection microscopy using diffracted beams. Ultramicroscopy, 1:145–150.

Cowley, J.M., and Moodie, A.F. (1957) The scattering of electrons by atoms and crystals. I. A new theoretical approach. Acta Crystallogr., 10:609–619.

Cowley, J.M., and Moodie, A.F. (1959a) The scattering of electrons by atoms and crystals. II. The effects of finite source size. Acta Crystallogr., 12:353–359.

Cowley, J.M., and Moodie, A.F. (1959b) The scattering of electrons by atoms and crystals. III. Single-crystal diffraction patterns. Acta Crystallogr., 12:360–375.

Darwin, C.G. (1914) Theorie dur Dispersion, Reflection und Brechung. Philos. Mag., 27:315–333, 675–690.

Fert, C., and Saport, R. (1952) Electron microscopy of reflection. Acad. Sci. Paris, 235:1490–1492.

Gaskill, J.D. (1978) Linear System, Fourier Transforms. John Wiley & Sons, Inc., New York, pp. 364–366.

Gotoh, Y., and Ino, S. (1978) Surface structure of Ag on Si (111) surface investigated by RHEED. J. Appl. Phys. Jpn., 17:2097–2109.

Harris, J.J., Joyce, B.A., and Dobson, P.J. (1981a) Oscillations in the surface structure of Sn-doped GaAs during growth by MBE. Surface Sci., 103:L90–96.

Harris, J.J., Joyce, B.A., and Dobson, P.J. (1981b) Comments on RED intensity oscillations during MBE of GaAs. Surface Sci., 108:L444–446.

Hojlund Nielsen, P.E., and Cowley, J.M. (1976) Surface imaging using diffracted electrons. Surface Sci., 54:340–354.

Houzay, F., Moison, J.M., and Bensoussan, M. (1984) Aluminum growth on (100) indium phosphide. J. Vac. Sci. Technol., B3:756–759.

Hsu, T. (1983) Reflection electron microscopy (REM) of vicinal surfaces of fcc metals. Ultramicroscopy, 11:167–172.

Hsu, T., and Cowley, J.M. (1983) Reflection electron microscopy (REM) of fcc metals. Ultramicroscopy, 11:239–250.

Hsu, T., Iijima, S., and Cowley, J.M. (1984) Atomic and other structures of cleaved GaAs (110) surfaces. Surface Sci., 137:849–856.

Ino, S. (1977) Some new techniques in reflection high energy electron diffraction (RHEED) application to surface structure studies. J. Appl. Phys. Jpn., 16:891–908.

Ino, S. (1980) An investigation of the Si (111) 7 × 7 surface structure by RHEED. J. Appl. Phys. Jpn., 19:1277–1290.

Ishizuka, and Uyeda, R. (1977) Acta Crystallogr., 833:740–749.

Kainuma, Y., and Uyeda, R. (1950) On the structure of adsorbed organic long-chain molecules on the cleavage surface of molybdenite. J. Phys. Soc. Jpn., 5:199–200.

Kawamura, T., Ohkawa, Y., and Miyake, S. (1976) The temperature effect and surface state resonance in medium energy electron diffraction by crystal. J. Phys. Soc. Jpn., 40:226–232.

Kohra, K., Moliere, K., Nakano, S., and Ariyama, M. (1962) Anomalous intensity of mirror reflection from the surface of a single crystal. J. Phys. Soc. Jpn., 17(Suppl.):82–85.

Lehmpfuhl, G., and Uchida, Y. (1988) Electron diffraction conditions for surface imaging. Ultramicroscopy, 26:177–188.

Ma, Y. (1989) Dynamical theory for high energy electron reflection. PhD thesis at Northwestern University, Evanston, Illinois, pp. 37–43, 71–78.

Ma, Y., and Marks, L.D. (1990) A robust solution for RHEED. Acta Crystallogr., in press.

Ma, Y., and Marks, L.D. (1989) Bloch-wave solution in the Bragg case. Acta Crystallogr., A45:174–182.

Ma, Y., and Marks, L.D. (1990a) Bloch waves and multislice in transmission and reflection diffraction. Acta Crystallogr., A46:11–32.

Ma, Y., and Marks, L.D. (1990b) Surface phenomena in RHEED and RHEEM. Acta Crystallogr., A46:594–606.

Maksym, P.A., and Beeby, J.L. (1981) A theory of RHEED. Surface Sci., 110:423–436.

Marks, L.D., and Ma, Y. (1989) Current flow in reflection electron microscopy and RHEED. Acta Crystallogr., A44:392–393.

Menter, J.W. (1953) Direct observation of solid surfaces at high resolution by reflection electron microscopy. J. Photo. Sci., 1:12–20.

Metherell, A.J. (1975) In: Electron Microscopy in Materials Science. U. Valdre and E. Ruedl, eds. Vol. 2:401–550.

Miyake, S. (1937a) Study of oxide films on metal surface with cathode-ray diffraction. II. Iron, chromium, nickel and their alloy. Sci. Pap. Inst. Phys. Chem. Res. (Tokyo), 31:161–173.

Miyake, S. (1937b) Electron diffraction by oxides of antimony formed on stibnate. Sci. Pap. Inst. Phys. Chem. Res. (Tokyo), 34:565–583.

Miyake, S., Kohra, K., and Takagi, M. (1954) The nature of the specular reflection of electrons from a crystal surface. Acta Crystallogr., 7:393–401.

Moon, A.R. (1972) Calculation of reflected intensities for medium and high energy electron diffraction. Z. Naturforsch., 27a:390–395.

Nishikawa, S., and Kikuchi, S. (1928a) Diffraction of cathode rays by mica. Nature, 121:1019–1020.

Nishikawa, S., and Kikuchi, S. (1928b) Diffraction of cathode rays by calcite. Nature, 122:726.

Osakabe, N., Tanishiro, Y., Yagi, K., and Honjo, G. (1980) Reflection electron microscopy by clean and gold deposited (111) silicon surfaces. Surface Sci., 97:393–408.

Osakabe, N., Tanishiro, Y., Yagi, K., and Honjo, G. (1981a) Image contrast of dislocations and atomic steps on (111) silicon surface in reflection electron microscopy. Surface Sci., 102:424–442.

Osakabe, N., Tanishiro, Y., Yagi, K., and Honjo, G. (1981b) Direct observation of the phase transition between the (7 × 7) and (1 × 1) structures of clean (111) silicon surfaces. Surface Sci., 109:353–366.

Peng, L.M., and Cowley, J.M. (1986) Dynamical diffraction calculation for RHEED and REM. Acta Crystallogr., A42:545–552.

Peng, L.M., and Cowley, J.M. (1988) A multislice approach to the RHEED and REM calculation. Surface Sci., 199:609–622.

Pukite, P.R., and Cohen, P.I. (1987) Multilayer steps formation after As adsorption on Si (100): Nucleation of GaAs on vicinal Si. Appl. Phys. Lett., 50:1739–1741.

Pukite, P.R., Van Hove, J.M., and Cohen, P.I. (1983) Sensitive reflection high-energy electron diffraction measurement of the local misorientation of vicinal GaAs surfaces. Appl. Phys. Lett., 44:456–458.

Ruska, E. (1933) Image of surfaces which reflect electrons in the electron microscope. Z. Phys., 83:492–497.

Self, P.G., O'Keefe, M.A., Buseck, P.R., and Spargo, A.E.C. (1983) Practical computation of amplitudes and phases in electron diffraction. Ultramicroscopy, 11:25–32.

Shimizu, N., Tanishiro, Y., Kobayshi, K., Takayanagi, K., and Yagi, K. (1985) Reflection electron microscopy study of the initial stages of oxidation of Si (111) 7 × 7 surfaces. Ultramicroscopy, 18:453–462.

Shimizu, N., Tanishiro, Y., Takayanagi, K., and Yagi, K. (1987) On the vacancy formation and diffusion on the Si (111) 7 × 7 surfaces under exposures of low oxygen pressure studies by the in situ reflection electron microscopy. Surface Sci., 191:28–44.

Uchida, Y., Jager, J., and Lehmpfuhl, G. (1984a) Direct imaging of atomic steps in reflection electron microscopy. Ultramicroscopy, 13:325–328.

Uchida, Y., and Lehmpfuhl, G. (1987a) Observation of double contours of monatomic steps on single crystal surfaces in reflection electron microscopy. Ultramicroscopy, 23:53–60.

Uchida, Y., and Lehmpfuhl, G. (1987b) Reflection electron microscopic observation of crystal surfaces on a Si cylindrical specimen. Surface Sci., 188:364–377.

Uchida, Y., Lehmpfuhl, G., and Jager, J. (1984b) Observation of sur-

face treatments on single crystals by reflection electron microscopy. Ultramicroscopy, 15:119–130.

Uyeda, R. (1940) Cathode-ray investigation of thin layers formed on some single crystals. III. Silver film on sulfide crystals. Proc. Phys.-Math. Soc. Jpn., 22:1023–1033.

Wood, C.E.C. (1981) RED intensity oscillations during MBE of GaAs. Surface Sci., 108:L441–443.

Yao, N., and Cowley, J.M. (1988) Characterization of double contours and twin images in REM. Proc. 46th Annu. Meeting EMSA. pp. 686–687.